The ejected mass distribution of type Ia supernovae:
A significant rate of non-Chandrasekhar-mass progenitors

R. A. Scalzo[1,2*], A. J. Ruiter[1,2,3], and S. A. Sim[2,4]

[1] *Research School of Astronomy and Astrophysics, Australian National University, Canberra, ACT 2611, Australia*
[2] *ARC Centre of Excellence for All-Sky Astrophysics (CAASTRO)*
[3] *Max-Planck-Institut für Astrophysik, Karl-Schwarzschild-Str. 1, 85741 Garching bei München, Germany*
[4] *Astrophysics Research Centre, School of Mathematics and Physics, Queen's University Belfast, Belfast, BT7 1NN, UK*

29 August 2014

ABSTRACT

The ejected mass distribution of type Ia supernovae directly probes progenitor evolutionary history and explosion mechanisms, with implications for their use as cosmological probes. Although the Chandrasekhar mass is a natural mass scale for the explosion of white dwarfs as type Ia supernovae, models allowing type Ia supernovae to explode at other masses have attracted much recent attention. Using an empirical relation between the ejected mass and the light curve width, we derive ejected masses M_{ej} and ^{56}Ni masses M_{Ni} for a sample of 337 type Ia supernovae with redshifts $z < 0.7$ used in recent cosmological analyses. We use hierarchical Bayesian inference to reconstruct the joint M_{ej}-M_{Ni} distribution, accounting for measurement errors. The inferred marginal distribution of M_{ej} has a long tail towards sub-Chandrasekhar masses, but cuts off sharply above 1.4 $M_\odot$. Our results imply that 25%–50% of normal type Ia supernovae are inconsistent with Chandrasekhar-mass explosions, with almost all of these being sub-Chandrasekhar-mass; super-Chandrasekhar-mass explosions make up no more than 1% of all spectroscopically normal type Ia supernovae. We interpret the type Ia supernova width-luminosity relation as an underlying relation between M_{ej} and M_{Ni}, and show that the inferred relation is not naturally explained by the predictions of any single known explosion mechanism.

Key words: white dwarfs; supernovae: general; cosmology: dark energy; methods: statistical

1 INTRODUCTION

Type Ia supernovae (SNe Ia) are widely used as distance indicators in cosmological studies of the dark energy (Riess et al. 1998; Perlmutter et al. 1999). Their accuracy and precision rely on empirical relations between their luminosity and their light curve width and colour, which suffice to establish luminosities to 15% and distances to 7% (Phillips 1993; Riess et al. 1996; Tripp 1998; Goldhaber et al. 2001). Other standardization methods have also been developed: reducing sensitivity to dust using intrinsic colours inferred from optical photometry several weeks past maximum light (Phillips et al. 1999; Conley et al. 2006; Folatelli et al. 2010) or from near-infrared photometry (Burns et al. 2014; Mandel et al. 2009, 2011); splitting the sample by spectroscopic properties (Wang et al. 2009; Foley & Kasen 2011); or using spectroscopic (Bongard et al. 2006; Chotard et al. 2011) or spectrophotometric (Bailey et al. 2009; Blondin et al. 2012) indicators instead of light curve parameters.

Despite the considerable attention devoted to type Ia supernovae in cosmology, the evolution of their progenitor systems, their

physical state at the time of explosion, and the explosion mechanisms are not fully understood (for recent reviews, see Wang & Han 2012; Hillebrandt et al. 2013; Ruiz-Lapuente 2014). The long-standing consensus holds that type Ia supernovae must result from the thermonuclear incineration of at least one carbon-oxygen white dwarf. This view is supported by several independent lines of evidence: the layered composition of SN Ia ejecta implied by their spectroscopic evolution, with iron-peak elements in the center and intermediate-mass elements such as silicon and sulfur on the outside (Stehle et al. 2005; Mazzali et al. 2007); the range of star formation histories in SN Ia host galaxies, showing that SNe Ia are not associated exclusively with young stars, as are other types of supernovae (Mannucci et al. 2006); and upper limits on the size of the progenitor, based on upper limits on shock breakout radiation (Piro et al. 2010) shortly after explosion for the very nearby SN 2011fe (Nugent et al. 2011; Bloom et al. 2012). SNe Ia also must result from interactions of the white dwarf with another star (e.g. Whelan & Iben 1973; Iben & Tutukov 1984), since an isolated white dwarf will simply cool and fade away over billions of years, and that a SN Ia progenitor is totally disrupted in the explosion, at least for the spectroscopically "normal" SNe Ia (Branch et al. 1993, 2006) used in cosmology.

---

* Email: rscalzo@mso.anu.edu.au

For a long time, the conventional wisdom has favored the delayed detonation (Khokhlov 1991) of a white dwarf near the Chandrasekhar mass $M_{\rm Ch} = 1.4\ M_\odot$ — a natural theoretical mass scale at which SNe Ia might explode — accreting and steadily burning material either from a non-degenerate (Whelan & Iben 1973) or white dwarf (Iben & Tutukov 1984) companion as the explosion mechanism for normal SNe Ia (Mazzali et al. 2007). However, recent indirect evidence suggests that this scenario cannot account for all normal SNe Ia. Such evidence includes the lack of observed X-ray emission (Gilfanov & Bogdan 2010) or ionized helium emission (Woods & Gilfanov 2013) associated with nuclear burning of accreted material on the surface of a white dwarf (see also Di Stefano 2010a,b), and the theoretical difficulty of accounting for observed SN Ia rates using only Chandrasekhar-mass white dwarfs (van Kerkwijk et al. 2010).

This pressure has motivated the study of other SN Ia channels in which the progenitor does not need to be very close to $M_{\rm Ch}$ for an explosion to take place. In such models, the ejected mass $M_{\rm ej}$ of a SN Ia encodes vital information about the progenitor evolution and explosion mechanism. They include: *double detonations*, in which a surface detonation drives a shock into the interior of a sub-Chandrasekhar-mass white dwarf and ignites it (Woosley & Weaver 1994; Fink et al. 2010); *spin-up/spin-down* models, in which angular momentum of accreted material enables a super-Chandrasekhar-mass white dwarf to support itself against explosion until internal stresses redistribute that angular momentum (Justham 2011; Di Stefano & Kilic 2012); *violent mergers* of two white dwarfs in which one or both white dwarfs explode shortly after the merger event (Pakmor et al. 2012), generally expected to be super-Chandrasekhar-mass; and *collisions* of two white dwarfs (Benz et al. 1989; Rosswog et al. 2009; Raskin et al. 2009) encouraged by Kozai resonances in triple systems (Thompson et al. 2011; Katz & Dong 2012; Hamers et al. 2013), which may have masses ranging from sub-Chandrasekhar to super-Chandrasekhar. Some spectroscopically peculiar, extremely luminous ($M_B \sim -20$) SNe Ia (Howell et al. 2006; Hicken et al. 2007; Yamanaka et al. 2009; Tanaka et al. 2010; Scalzo et al. 2010; Taubenberger et al. 2011, 2013). are interpreted as having ejected a super-Chandrasekhar mass of material. Mazzali et al. (2011) find a good fit to the nebular spectrum of the subluminous, but spectroscopically normal, SN Ia 2003hv using a sub-Chandrasekhar-mass model ejecting about $1.0\ M_\odot$; Mazzali & Hachinger (2012) make similar arguments for SN 1991bg. Mazzali et al. (2007) suggest a lower limit of about $1.0\ M_\odot$ on the mass ejected in a spectroscopically normal SN Ia.

In a similar vein, while improved luminosity standardization for cosmology remains an active area of research, the physical origin of the width-luminosity (or width-colour-luminosity) relation has yet to be fully understood. SNe Ia are powered by the radioactive decay chain $^{56}{\rm Ni} \to {}^{56}{\rm Co} \to {}^{56}{\rm Fe}$, as has now been directly confirmed by observation of gamma rays from this decay chain in the nearby SN 2014J (Churazov et al. 2014). The mass $M_{\rm Ni}$ of $^{56}{\rm Ni}$ synthesized in the explosion largely determines the peak bolometric luminosity ("Arnett's rule"; Arnett 1982) and hence is somehow linked with the light curve width. Possible physical drivers include changes in opacity with temperature (Khokhlov et al. 1993; Höflich & Khohklov 1996) or with synthesized total iron-peak element mass (Mazzali et al. 2007), variation of the overall ejected mass (Pinto & Eastman 2000), or asymmetries arising from hydrodynamic instabilities in three-dimensional explosion models (Woosley & Kasen 2007; Kasen et al. 2009). Improved understanding of the physics behind the width-luminosity relation would put the measurement of distances to SNe Ia on sound theoretical foot-

ing, and could uncover new luminosity correlates related to specific explosion mechanisms or progenitor channels. Many of the above-mentioned scenarios make predictions for $M_{\rm Ni}$, or equivalently the absolute magnitude, of a SN Ia as a function of progenitor mass.

Recently, Scalzo et al. (2014a) derived ejected masses for a sample of 19 spectroscopically normal SNe Ia observed by the Nearby Supernova Factory (SNfactory) by modeling their bolometric light curves. They found that normal SNe Ia show a range of ejected masses from 0.9–1.4 $M_\odot$, roughly compatible with the findings of Mazzali et al. (2007) and Mazzali et al. (2011), with about 15% systematic uncertainty on the absolute mass scale of the explosion. They also found a tight correlation between $M_{\rm ej}$, as derived from the bolometric light curve, and the light curve width x_1, as measured from multi-band photometry by the SALT2 cosmological light curve fitter (Guy et al. 2007, 2010). These findings confirm the earlier observational results of Stritzinger et al. (2006), using a similar technique, but with a factor of three improvement in the precision of the reconstruction. The method of Scalzo et al. (2014a) was validated using synthetic data from contemporary three-dimensional SN Ia explosion models, demonstrating the ability to distinguish between explosion scenarios based on the ejected mass.

In this paper, we interpret the SN Ia width-luminosity relation in terms of an underlying relation between $M_{\rm ej}$ and $M_{\rm Ni}$. We apply the Scalzo et al. (2014a) $M_{\rm ej}$-x_1 relation and a version of Arnett's rule to estimate $M_{\rm ej}$ and $M_{\rm Ni}$ for a large sample of SNe Ia with redshift less than 0.7. We then use hierarchical Bayesian inference to reconstruct the *joint $M_{\rm ej}$-$M_{\rm Ni}$ distribution* for this sample. This establishes a proof of principle for the direct comparison of observations with predicted theoretical distributions, based on our best contemporary binary population synthesis and numerical explosion models. Finally, we derive a relative rate of non-Chandrasekhar-mass SNe Ia based on this distribution and discuss the implications for the progenitor evolution and explosion mechanism(s).

2   HIERARCHICAL BAYESIAN INFERENCE OF THE JOINT $M_{\rm ej}$-$M_{\rm Ni}$ DISTRIBUTION

To derive an accurate $M_{\rm ej}$-$M_{\rm Ni}$ joint distribution, we require a pure, unbiased sample of spectroscopically normal SNe Ia. Numerous observational selection effects prevent any real sample from fully realizing this ideal. For our purposes, we require that the supernovae we use are spectroscopically confirmed *normal* SNe Ia that could appear in a cosmology analysis. We also require supernovae that have been discovered in a search not targeting specific host galaxies, to avoid environmental biases on the distribution of intrinsic SN Ia properties. The recent Joint Light Curve Analysis sample (JLA; Betoule et al. 2014), drawing from the untargeted SDSS (Frieman et al. 2008) and SNLS (Astier et al. 2006) searches, provides a good initial source of spectroscopically confirmed SNe Ia that have in fact been used in a cosmology analysis. We confine our attention to volume-limited subsamples of the Betoule et al. (2014) SNe Ia to avoid Malmquist bias on the light curve width and colour, and we include only SNe Ia that pass all of the Betoule et al. (2014) data quality cuts and have reliable SALT2 light curve fits. We select SDSS SNe with $z < 0.2$ (197 SNe) and SNLS SNe with $z < 0.7$ (140 SNe), for a total of 337 SNe Ia.

The JLA SNe Ia do not, in general, have sufficiently broad wavelength coverage in multi-band photometry to construct full bolometric light curves; while corrections can be made for missing ultraviolet and near-infrared flux, measurements equivalent to rest-frame $UBVRI$ are needed. They are also, in general, not observed out to the $^{56}{\rm Co}$-dominated phase needed to apply the full mass re-

construction method of Scalzo et al. (2014a). However, the correlation between $M_{\rm ej}$ and SALT2 x_1 found by Scalzo et al. (2014a) can be used to estimate $M_{\rm ej}$ without full bolometric light curves. The Scalzo et al. (2014a) SNe Ia also show a strong correlation between inferred $M_{\rm Ni}$ and absolute magnitude M_B, as expected from Arnett's rule. We can therefore use such relations to transform the SALT2 light curve fit parameters (m_B, x_1, c) directly into intrinsic properties $(M_{\rm ej}, M_{\rm Ni})$ within the JLA best-fitting cosmology.

To find the transformation equations, we perform least-squares fits using $M_{\rm ej}$ and $M_{\rm Ni}$ values from run F in table 6 of Scalzo et al. (2014a), including all spectroscopically normal SNe Ia and incorporating measurement errors in both the dependent and independent variables for each fit. We obtain

$$M_{\rm ej}/M_\odot = (1.322 \pm 0.022) + (0.185 \pm 0.018)\, x_1 \qquad (1)$$

with $\chi^2/\nu = 13.3/16 = 0.829$ and 6% RMS dispersion, and

$$\log M_{\rm Ni}/M_\odot = -0.4(M_B + 19.841 \pm 0.020) \qquad (2)$$

with $\chi^2/\nu = 3.794/16 = 0.237$ and 8% RMS dispersion. Here M_B has been corrected for host galaxy dust extinction assuming a Cardelli et al. (1988) extinction law with $R_V = 3.1$. The value of $M_{\rm Ni}$ from the full bolometric light curve fit can be even more accurately predicted (to 4% RMS) by adding to Equation 2 a term linear in extinction-corrected colour, i.e., a bolometric correction at maximum light. Such a correction requires an independent estimate of the dust extinction for each SN, which is problematic for the JLA sample. We can proceed using Equation 2 assuming a scenario similar to that studied by Scolnic et al. (2013), in which colour variation among SNe Ia is due almost entirely to dust with $R_V = 3.1$, and neglecting the bolometric correction. While by no means absolutely certain, there is some independent evidence that such a scenario may not be far from the truth (e.g., Chotard et al. 2011).

Multilinear regressions against all three SALT2 light curve variables do not significantly improve predictions for $M_{\rm ej}$ and $M_{\rm Ni}$ over these single-parameter relations. In other words, $M_{\rm ej}$ is most directly related to x_1, $M_{\rm Ni}$ is most directly related to M_B (after correction for extinction), and any other correlations, such as the width-luminosity relation itself, are secondary to these, at the level of detail of the Scalzo et al. (2014a) modeling. In general, the dominant uncertainties on $M_{\rm ej}$ and $M_{\rm Ni}$ are systematic, and are associated with limitations in the bolometric light curve modeling rather than observed scatter around these relations. The unknown functional form of the ejecta density profile is the largest driver of uncertainty in $M_{\rm ej}$; if it is the same for all SNe Ia, its first-order influence is to change the zeropoint of Equation 1, without affecting the slope or statistical significance. The largest uncertainty in $M_{\rm Ni}$ is the extent of radiation trapping near bolometric maximum light. This is represented by a factor α representing the ratio of the bolometric luminosity to the rate of energy input from radioactive decay, which may vary from SN to SN, but is believed to be close to 1 for a variety of explosion models (Arnett 1982; Khokhlov et al. 1993; Nugent et al. 1995; Höflich & Khokhlov 1996; Howell et al. 2009; Blondin et al. 2013).

Simply applying Equations 1 and 2 to determine $(M_{\rm ej}, M_{\rm Ni})$ from (m_B, x_1, c) for each SN, and propagating Gaussian uncertainties, produces an *observed* two-dimensional distribution that has been distorted by measurement errors. To infer the *error-free* distribution, we use the forward-modeling algorithm of Hogg et al. (2010). This is an importance-sampling method that requires samples from the $(M_{\rm ej}, M_{\rm Ni})$ joint probability distribution for each SN Ia. We first generate (M_B, x_1, c) samples using (the Cholesky decomposition of) the covariance matrix of the SALT2 light curve fit for each SN as given in Betoule et al. (2014). Inspired by the

BALT prescription of Scolnic et al. (2013), we interpret variation in c as due entirely to dust extinction with $R_V = 3.1$, with

$$P(c) = e^{-(c-\bar{c})^2/\tau_S^2} \qquad (3)$$

for $c > \bar{c}$, with $\bar{c} = -0.1$ and $\tau_S = 0.11$. We impose this prior by random rejection of samples as they are generated. After applying the extinction correction to M_B for each sample, we use Equations 1 and 2 to convert (x_1, M_B) directly to $(M_{\rm ej}, M_{\rm Ni})$. We apply an additional 6% random Gaussian scatter to $M_{\rm ej}$ after sampling, to represent dispersion of the results from the full bolometric light curve fit around Equation 1. We also apply an additional 20% random Gaussian scatter to $M_{\rm Ni}$, to represent potential variation in the radiation trapping factor α between different SNe Ia, typical of the priors used in Scalzo et al. (2014a). Equation 2 assumes $\alpha = 1$, and while M_B is a good predictor of bolometric luminosity for SNe Ia, the true spread in $M_{\rm Ni}$ may be larger than what we infer.

We parametrize the intrinsic $(M_{\rm ej}, M_{\rm Ni})$ distribution as a sum of Gaussians, centered on a grid with $0.7 < M_{\rm ej}/M_\odot < 1.7$ (spacing 0.05) and $0.3 < M_{\rm Ni}/M_\odot < 0.8$ (spacing 0.1), with width in each direction equal to the grid spacing, resulting in 100 parameters (the "bin" heights). For each SN Ia, we draw $k = 200$ samples $(M_{\rm ej}, M_{\rm Ni})$ based on the SALT2 light curve fit, and use these to calculate the Hogg et al. (2010) likelihood for the parameters describing the intrinsic distribution. We minimize this likelihood to provide a plausible initial guess for the form of the intrinsic distribution, then sample the full joint distribution of the parameters using the affine-invariant Markov chain Monte Carlo code EMCEE (Foreman-Mackey et al. 2013).

Once we have inferred the intrinsic distribution $P(M_{\rm ej}, M_{\rm Ni})$, we can re-apply it as a prior to find new, hierarchical estimates for $M_{\rm ej}$ and $M_{\rm Ni}$ for each SN Ia. The bolometric light curve fits in Scalzo et al. (2014a) incorporated knowledge of SN Ia explosion physics into the likelihood $P({\rm data}|M_{\rm ej}, M_{\rm Ni})$, including constraints between $M_{\rm ej}$, $M_{\rm Ni}$, and other nuisance parameters such as the kinetic energy of the explosion; however, they used an uninformative (uniform) prior $P_0(M_{\rm ej}, M_{\rm Ni})$. We can thus approximate

$$P(M_{\rm ej}, M_{\rm Ni}|{\rm data}) = \frac{P({\rm data}|M_{\rm ej}, M_{\rm Ni})\, P(M_{\rm ej}, M_{\rm Ni})}{P({\rm data})} \qquad (4)$$

by re-weighting the $(M_{\rm ej}, M_{\rm Ni})$ samples for each SN Ia by the inferred $P(M_{\rm ej}, M_{\rm Ni})$. While single-point estimates use only information about the light curve, the hierarchical estimate incorporates information about where the other SNe Ia in the sample are found in the $(M_{\rm ej}, M_{\rm Ni})$ plane. The distribution of hierarchical estimates is more concentrated than the inferred error-free distribution because of the measurement uncertainties in the individual points; in the limit of large errors, the posterior probability for each SN simply becomes the prior.

Figure 1 shows joint confidence regions in the $(M_{\rm ej}, M_{\rm Ni})$ plane for the combined sample, bounded by level sets of probability density, together with the best estimate of these parameters (and uncertainties) for each supernova. The predictions of two contemporary explosion models are also shown: double detonations (Fink et al. 2010) and white dwarf collisions (Kushnir et al. 2013). The red dot-dashed line shows the transformation into the $M_{\rm ej}$-$M_{\rm Ni}$ plane of the best-fitting SN Ia M_B-x_1 relation from Betoule et al. (2014), which the hierarchical estimates for each SN Ia trace with about 8% dispersion in $M_{\rm Ni}$; this is of a similar order to the dispersion found by Scolnic et al. (2013) under similar assumptions about SN Ia intrinsic colour and extinction. At this level of detail, the relation still appears to be a single-parameter family, with no clear evidence for multiple sub-populations with different explosion properties (e.g. different intrinsic luminosities).
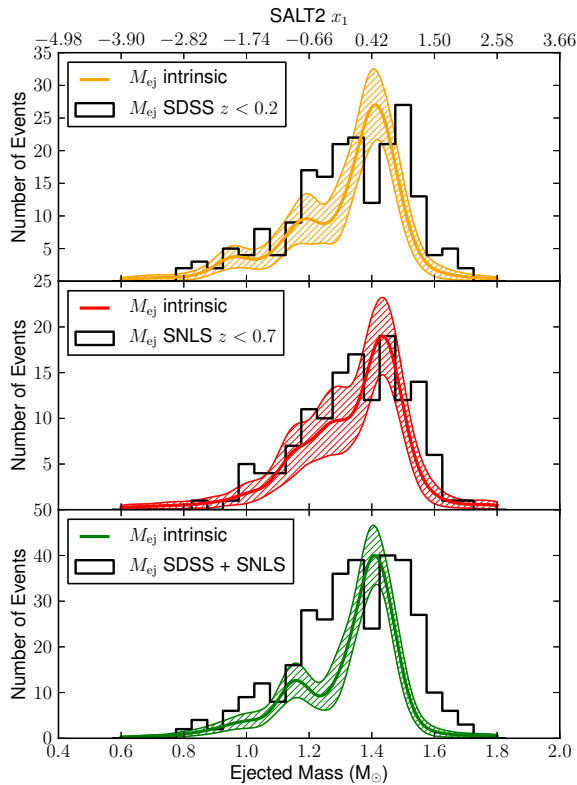
Figure 2. Marginal distribution of M_{ej} over subsets of SNe Ia used in the Betoule et al. (2014) cosmological analysis. Top: SDSS SNe Ia with $z < 0.2$. Middle: SNLS SNe Ia with $z < 0.7$. Bottom: Union of the two subsets. Histograms show the original distribution of mean values as inferred directly from the SALT2 light curve parameters. Coloured curves with hatched bands show the mean and 68% CL variation of the intrinsic distribution, parametrized as a sum of Gaussians.

For a simpler view, Figure 2 shows the marginal distributions of M_{ej} inferred separately from the SDSS, SNLS, and combined samples. The marginal M_{ej} distributions show that the distribution of x_1 for SDSS supernovae is similar to that for SNLS supernovae. Both distributions show a tail towards lower M_{ej}, and both show a sharp cutoff of the distribution above about 1.45 $M_{\odot}$. The peak of the marginalized M_{ej} distribution is close to 1.4 $M_{\odot}$. The hint of structure at around 1.2 $M_{\odot}$ is tantalizing, but not highly statistically significant; we discuss the possible implications in §4 below.

We caution that these results rely on the accuracy of the assumptions of Scalzo et al. (2014a), from which Equations 1 and 2 were derived: spherically symmetric ejecta, with a stratified composition and a universal functional form for the radial density profile, for all normal SNe Ia. While these properties agree with conventional wisdom for the modeling of SN Ia explosions and can be supported observationally, there may be variation among real SNe Ia that is not captured by our model. Scalzo et al. (2014a) had some difficulty accurately reproducing M_{Ni} for some highly asymmetric SN Ia explosion models, although inferred M_{Ni} tracks modeled M_{Ni} for angle-averaged light curves. Similarly, if the ejecta density profiles of SNe Ia vary systematically with light curve width, this could affect the slope of Equation 1 and hence the shapes of our inferred distributions.
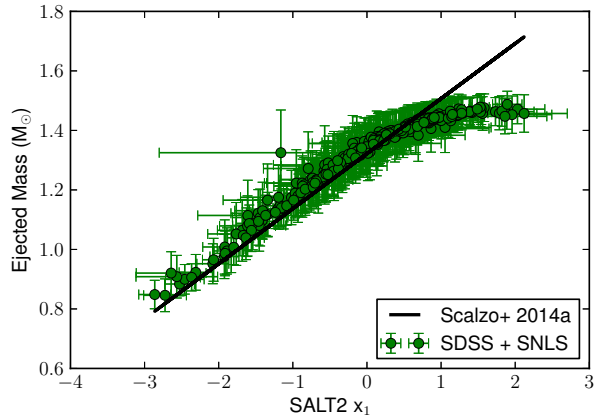

Figure 3. The M_{ej}-x_1 relation for our sample. Symbols with error bars are hierarchical Bayesian estimates for individual SNe Ia as shown in Figure 1. Solid line: Equation 1.

3   RELATIVE RATES OF NON-CHANDRASEKHAR-MASS SNE IA

The calibration of the zeropoint of Equation 1 is also subject to uncertainty at the 10–15% level (Scalzo et al. 2014a). In this context, the sharp peak in our inferred distribution of M_{ej} at 1.4 $M_{\odot}$ carries weight in any physical interpretation of the distribution. Scalzo et al. (2014a) present strong evidence that SNe Ia do not all explode at M_{Ch}. However, if the calibration of our ejected mass scale is very far from what we assume, we then have the additional challenge of explaining why most SNe Ia explode at a preferred mass *other* than M_{Ch}. Some theoretical scenarios, such as the double-degenerate violent merger scenario, may provide motivation for such a peak; we discuss these cases in §4.

Figure 3 shows how the functional dependence of M_{ej} on x_1 changes when the prior $P(M_{ej}, M_{Ni})$ is taken into account. We see that the Scalzo et al. (2014a) M_{ej}-x_1 relation changes little for SNe with $x_1 < +0.5$, although it underestimates the mass slightly relative to the hierarchical estimate, since faster-declining SNe Ia are intrinsically less numerous. For slower-declining supernovae, the relation begins to flatten until it is consistent with a constant ($M_{ej} = 1.45 \ M_{\odot}$) for all SNe Ia with $x_1 > +1$. The spectroscopically peculiar 1991T-like SNe Ia are usually found in this range: SN 1991T (Filippenko et al. 1992; Phillips et al. 1992), SN 2003fg (SNLS-03D3bb; Howell et al. 2006), SN 2007if (Scalzo et al. 2010; Yuan et al. 2010), LSQ12gdj (Scalzo et al. 2014b), and three of the five additional super-Chandrasekhar-mass SN Ia candidates considered in Scalzo et al. (2012) have $x_1 > +1$, and among these only SN 2003fg and SN 2007if have been established as having super-Chandrasekhar-mass ejecta at high confidence. Since the 1991T-like sub-classification becomes less secure in post-maximum spectra Li et al. (2011), it is possible that some of these very-slowly-declining SNe Ia are actually 1991T-like.

We can make a very conservative estimate of the relative rate of non-M_{Ch} explosions by considering only *individual* SNe Ia which are incompatible with a Chandrasekhar-mass explosion, based on the hierarchical Bayesian estimates of M_{ej} and M_{Ni}. We estimate errors in the relative rates by drawing samples $P_j(M_{ej}, M_{Ni})$ from the posterior for the inferred $P(M_{ej}, M_{Ni})$, and using these to make different realizations of the hierarchical estimates for each SN. Out of 337 SNe Ia, we find 93.6 ± 13.2, or $(27.8 \pm 3.9)\%$, have $M_{ej} < M_{Ch}$ at 95% CL or greater; in contrast, only 4.5 ± 1.4, or $(1.3 \pm 0.4)\%$, have $M_{ej} > M_{Ch}$ at 95% CL or greater. The boundary between Chandrasekhar-mass
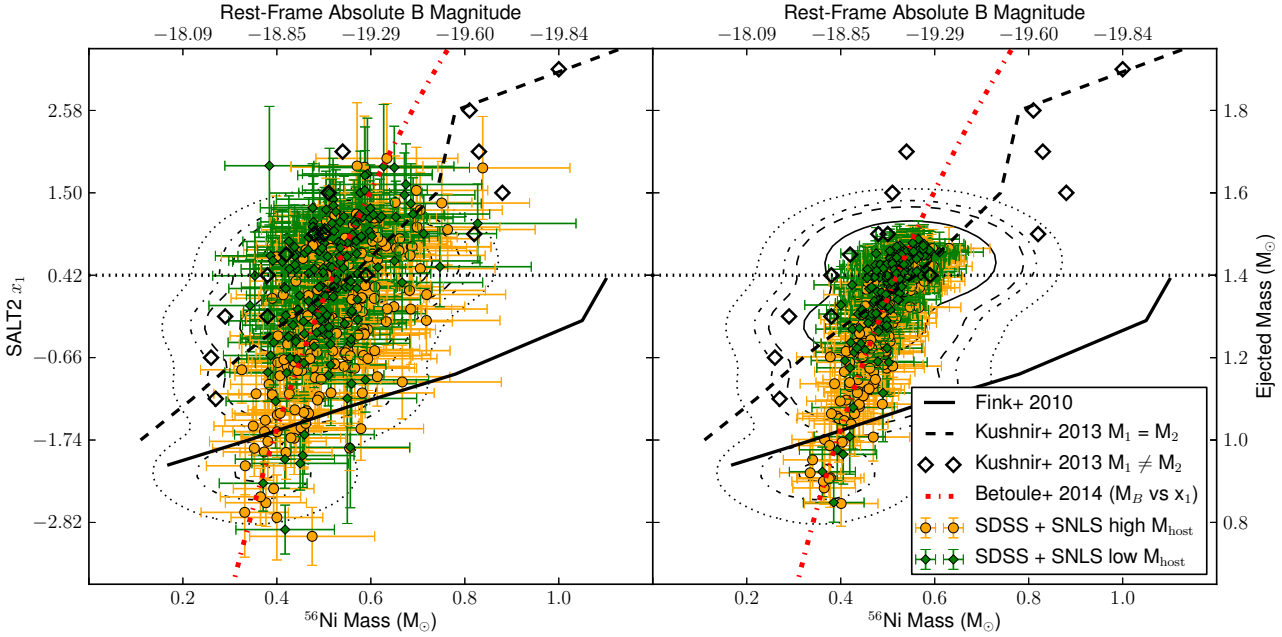
Figure 1. Joint $M_{\rm ej}$-$M_{\rm Ni}$ distribution for 337 SNe Ia. Black open diamonds: non-equal-mass white dwarf collisions of Kushnir et al. (2013). Dashed line: equal-mass white dwarf collisions of Kushnir et al. (2013). Solid line: double detonations of Fink et al. (2010). Contours: 68%, 90%, 95%, and 99% confidence regions, bounded by level sets of probability density, for the $M_{\rm ej}$-$M_{\rm Ni}$ distribution. Symbols with error bars: Bayesian mass estimates for individual SNe Ia (green: $M_{\rm host} < 10^{10} M_{\odot}$; orange: $M_{\rm host} > 10^{10} M_{\odot}$). Left: estimates of $M_{\rm ej}$ and $M_{\rm Ni}$ using Equations 1 and 2 with an uninformative prior $P_0(M_{\rm ej}, M_{\rm Ni})$; right: imposing as a prior the inferred joint $M_{\rm ej}$-$M_{\rm Ni}$ distribution $P(M_{\rm ej}, M_{\rm Ni})$ shown by the contours (right).

and sub-Chandrasekhar-mass systems is thus two standard deviations from 1.4 $M_{\odot}$, or about 1.23 $M_{\odot}$ assuming 6% dispersion around Equation 1.

For a more realistic estimate of the *total* number of non-Chandrasekhar-mass SNe Ia, we set plausible boundaries for the Chandrasekhar-mass regime based on explosion physics, and then count the number of SNe Ia lying outside this region; individual SNe Ia can scatter either into this region or out of it, based on measurement errors. With regard to the lower mass bound, Lesaffre et al. (2006) simulate the evolution of accreting white dwarfs through the carbon flash, and find ignition takes place at central densities above 2×10^9 g cm^{-3}. In three-dimensional simulations of Chandrasekhar-mass delayed detonations, Seitenzahl et al. (2011) and Krueger et al. (2012) consider central densities as low as 10^9 g cm^{-3}, corresponding to a mass of 1.36 $M_{\odot}$ for a non-rotating white dwarf. On the high-mass end, white dwarfs in rigid rotation could be as massive as 1.5 $M_{\odot}$ (Anand 1965; Roxburgh 1965); white dwarfs more massive than this would correspond to the super-Chandrasekhar-mass, differentially rotating white dwarfs of Yoon & Langer (2005).

We therefore take $1.35 < M_{\rm ej}/M_{\odot} < 1.5 M_{\odot}$ to be "Chandrasekhar-mass" — massive enough to ignite spontaneously, but still close to the rigidly rotating regime. These boundaries yield 174.1 ± 15.2 Chandrasekhar-mass, 159.8 ± 15.1 sub-Chandrasekhar-mass, and 3.1 ± 0.9 super-Chandrasekhar-mass events, or a sub-Chandrasekhar-mass rate of (47.4 ± 4.5)%.

Both of these relative rate estimates are consistent with the expectation that sub-Chandrasekhar-mass SNe Ia are relatively common (Scalzo et al. 2014a), while super-Chandrasekhar-mass SNe Ia are quite rare (Scalzo et al. 2012). Thus, if the peak of our derived $M_{\rm ej}$ distribution actually occurs at $M_{\rm Ch}$, 25%–50% of all normal SNe Ia eject sub-Chandrasekhar masses. This number can increase

if our absolute mass scale is miscalibrated and the peak in the distribution represents a lower mass.

4 INTERPRETING THE JOINT $M_{\rm ej}$-$M_{\rm Ni}$ DISTRIBUTION

The identification of ejected mass as the primary factor determining light curve shape provides a fresh interpretation of previous work on SN Ia progenitors and their evolution over cosmic time, a few examples of which we give here. SN Ia rates (Scannapieco et al. 2005) and delay time distributions (Mannucci et al. 2006) are explained well by models with two populations of SNe Ia, split by host galaxy properties such as stellar mass and star formation rate (Sullivan et al. 2006) and metallicity (Howell et al. 2009). Howell et al. (2009) found that fast-declining (SALT1 $s < 0.9$, SALT2 $x_1 < -0.9$) SNe Ia happen almost exclusively in high-metallicity galaxies ($12 + \log({\rm O/H}) > 8.8$); these correspond to SNe Ia with $M_{\rm ej} < 1.15 M_{\odot}$, and we see a related preference of these SNe Ia for high-mass (metal-rich, old, passive) galaxies in our Figure 1. Howell et al. (2007) investigated the possible evolution of the light curve width with redshift; figure 2 of that work maps directly on to our Figure 2, although we find a less pronounced evolution trend. The $z < 0.1$ sample of Howell et al. (2007) was drawn from targeted searches that sampled different host galaxy environments from the untargeted SDSS and SNLS searches, which may be enough to explain the discrepancy.

Piro et al. (2014) considered different possible theoretical forms of an underlying $M_{\rm ej}$-$M_{\rm Ni}$ relation, motivated by the same explosion models we consider here. However, Piro et al. (2014) compared to data by using the width-luminosity relation to transform light curve width Δm_{15} to $M_{\rm Ni}$ (Mazzali et al. 2007), then transforming $M_{\rm Ni}$ to $M_{\rm ej}$ assuming that all SNe Ia come from a single explosion mechanism. Our work goes beyond this by providing more direct estimates of both $M_{\rm ej}$ and $M_{\rm Ni}$, and by estimating

the actual relative rate of SNe Ia inconsistent with Chandrasekhar-mass delayed detonations (which thus *require* an explanation by some alternative scenario). Our framework also enables comparison to explosion scenarios that predict only a M_{ej}-M_{Ni} joint distribution rather than a one-to-one relation; this may be useful when including uncertainties in ^{56}Ni production mentioned by Piro et al. (2014), e.g., impact parameters in white dwarf collisions.

In this section we consider the specific implications of our findings for a range of explosion scenarios. Different uncertainties in our analysis of $P(M_{ej}, M_{Ni})$ have different impacts on particular explosion models, which we include in our discussion.

4.1   Chandrasekhar-mass delayed detonations

A large relative rate of Chandrasekhar-mass SNe Ia would readily explain the peak we observe in the M_{ej} distribution near 1.4 $M_{\odot}$. In fact, conventional Chandrasekhar-mass scenarios are the *only* known progenitor scenario that naturally result in such a peak, providing a strong motivation to believe that they contribute significantly to the overall SN Ia rate. In addition, Seitenzahl et al. (2013b) showed that a large fraction ($\sim$ 50%) of SNe Ia must explode at or near M_{Ch} in order to explain the solar abundance of manganese observed in the Galaxy. The best-studied explosion mechanism in this case is a delayed detonation, taking place within the single-degenerate scenario.

In the single-degenerate scenario, a white dwarf accretes from a disc fed by Roche lobe overflow from a binary companion (Whelan & Iben 1973). As it accretes mass, the white dwarf primary must therefore also accrete angular momentum. This will tend to increase its rotation rate and support it against collapse or explosion. Thus the Chandrasekhar-mass scenario could, with little modification, account for a modest range of M_{ej}, e.g. 1.4–1.5 $M_{\odot}$ for solid-body rotation (Anand 1965; Roxburgh 1965). There are arguments that differentially rotating white dwarfs should not occur in nature (e.g., Piro et al. 2008), but if it does occur, similar explosion scenarios could be realized for higher, super-Chandrasekhar masses (Justham 2011; Hachisu et al. 2011; Di Stefano & Kilic 2012). Within this picture, ^{56}Ni production would have to be controlled by some other parameter, to account for the $\sim$ 0.2 $M_{\odot}$ spread in M_{Ni} for systems with ejecta mass near M_{Ch}. This can be fairly easily achieved in model sequences that vary properties of the ignition or the transition to detonation (Kasen et al. 2009; Seitenzahl et al. 2013a; Sim et al. 2013).

However, Chandrasekhar-mass explosions cannot explain all SNe Ia if M_{ej} is linked directly to light curve shape. Scalzo et al. (2014a) discuss the limitations of the original bolometric light curve modeling on which Equations 1 and 2 is based. The challenge in reproducing a normal SN Ia with a fast-declining (SALT2 $x_1 < -1$) light curve with a Chandrasekhar-mass model is to ensure that the decline from maximum to late times (> 60 days after explosion) is also adequately reproduced. Reducing the Compton depth by shifting ^{56}Ni to higher velocities, e.g., by displacing ^{56}Ni with stable iron as a result of neutronization (Höflich et al. 2004; Motohara et al. 2006), is not sufficient to do this; a substantial fraction of ^{56}Ni at high velocities would be needed.

Alternatively or in addition, the radiation-trapping factor α could be much greater than 1; reproducing the Scalzo et al. (2014a) bolometric light curve of SN 2008ec, for instance, would require $\alpha > 1.5$. For centrally concentrated ^{56}Ni and constant opacity, $\alpha = 1$, and shifting ^{56}Ni outwards tends to reduce α (Pinto & Eastman 2000). In the context of 1-D models, the same factors that increase α also tend to increase the diffusion time. A rapid release of trapped energy could in principle be achieved by

a dramatic drop in the opacity before or near maximum light, perhaps driven by cooling of the ejecta (Khokhlov et al. 1993), but a large effect is needed. Blondin et al. (2013), using the detailed radiation-transfer code CMFGEN, in fact find little dependence of α on M_{Ni} for a sequence of 1-D Chandrasekhar-mass delayed detonations; they also find broader bolometric light curves for SNe Ia with less ^{56}Ni, in contrast to what Scalzo et al. (2014a) observe (see figure 6 of the latter paper). Finally, highly aspherical ejecta can produce large variations in the maximum-light bolometric luminosity depending on the viewing angle, but these effects occur more often in non-Chandrasekhar-mass models such as violent mergers (Pakmor et al. 2012; Moll et al. 2014), and the low continuum polarization of most SNe Ia argues against highly aspherical explosions (Wang & Wheeler 2008).

Explosions at or near the Chandrasekhar mass limit might also result from white dwarfs fed by accretion of material from a disrupted white dwarf secondary, resulting from a massive double-degenerate merger event (Iben & Tutukov 1984). In this case, the ejected mass may exceed M_{Ch} when the mass of the secondary is included. However, it may be more likely that the final result of such a merger is collapse to a neutron star, rather than explosion (Nomoto & Kondo 1991). Moreover, simulations of supernovae surrounded by dense carbon-oxygen envelopes, as might arise from such mergers, result in explosions that may not resemble normal SNe Ia (Fryer et al. 2010; Blinnikov & Sorokina 2010).

4.2   Chandrasekhar-mass pure deflagrations

Pure deflagrations present a mechanism to produce weak explosions of Chandrasekhar-mass progenitors, possibly leaving a bound remnant (Livne et al. 2005). Simulations of pure deflagrations in Chandrasekhar-mass white dwarfs have recently been carried out by Jordan et al. (2012) and by Fink et al. (2014). These simulated explosions predict a mean trend in which M_{ej} varies significantly with moderate change in M_{Ni}; for example, Table 1 of Fink et al. (2014) shows models with $0.86 < M_{ej}/M_{\odot} < 1.4$ and $0.26 < M_{Ni}/M_{\odot} < 0.38$. However, deflagrations with bound remnants produce too little ^{56}Ni to explain observations of normal SNe Ia. Additionally, synthetic observables (light curves and spectra) for these models have been shown to give a poor match to normal SNe Ia; instead they match fairly well to observations of the members of the peculiar class of 2002cx-like SNe Ia (Jha et al. 2006; Phillips et al. 2007; Kromer et al. 2013a; Long et al. 2013). Sahu et al. (2008) find that observations of the 2002cx-like SN Ia 2005hk is consistent with a Chandrasekhar-mass pure deflagration in which the white dwarf is completely disrupted, leaving no remnant.

In any event, pure deflagrations are at present being invoked to explain spectroscopically peculiar, underluminous SNe Ia with low explosion energy, rather than spectroscopically normal SNe Ia appearing on the Hubble diagram. We therefore consider it unlikely that Chandrasekhar-mass pure deflagrations have an important role in explaining the joint M_{ej}-M_{Ni} distribution in Figure 1.

4.3   Sub-Chandrasekhar-mass double detonations

Detonations of sub-Chandrasekhar-mass white dwarfs can produce bright explosions (high M_{Ni}) for relatively low M_{ej}. A detonation of a hydrostatic carbon-oxygen white dwarf with mass in the range 1.0–1.15 $M_{\odot}$ will completely unbind the white dwarf and yield ^{56}Ni mass in a range that brackets the values inferred for our sample of objects (Sim et al. 2010). Synthetic light curves and spectra for such explosions provide a reasonable match to the properties

of normal SNe Ia near maximum light (Sim et al. 2010), adding weight to the possibility that sub-Chandrasekhar-mass detonations might produce normal SNe Ia in nature.

The best known sub-Chandrasekhar-mass explosion scenario is the *double-detonation* scenario, in which detonation of a helium layer on the surface of a carbon-oxygen white dwarf drives a compression shock into the white dwarf's interior, eventually causing it to detonate in turn (Woosley & Weaver 1994; Fink et al. 2010; Woosley & Kasen 2011). The necessary helium could be accreted slowly from a non-degenerate (Iben & Tutukov 1991) or degenerate (Ruiter et al. 2014) companion, or could arise from a merger with a helium white dwarf (Pakmor et al. 2013). The locus of points in Figure 1 with M_{ej} in the range 0.9–1.1 $M_\odot$ are consistent with the prediction of the double-detonation model of Fink et al. (2010). The apparent excess of events near this mass in Figure 2 could also arise from this channel, although future analyses with larger samples will clarify whether this excess is real.

However, the double-detonation scenario struggles to match the whole population or explain the joint distribution. A generic prediction of detonations in cold, hydrostatic white dwarfs is that M_{Ni} should be very sensitive to the progenitor mass, producing a steep dependence of M_{Ni} on M_{ej}. In contrast, our analysis suggests that M_{Ni} varies relatively weakly as a function of the ejected mass for SNe Ia in nature. Piro et al. (2014) make the similar point that only double detonations occurring in a very limited range of M_{ej} produce M_{Ni} consistent with normal SNe Ia. They suggest that the ^{56}Ni production in a double-detonation explosion may be sensitive to other factors depending on the dynamical details of the accretion or merger process (e.g., Zhu et al. 2013; Dan et al. 2013).

It is also conceivable, but unlikely, that the main peak in our inferred mass distribution actually occurs at a lower mass, due to modeling uncertainties as mentioned in §2. The ejecta density profiles for the faintest, fastest-declining SNe Ia in our distribution would have to be even more centrally peaked than an exponential to increase the Compton depth. This would bring our assumptions into tension with widths of nebular lines observed in SNe Ia ($\sim 10^4$ km s^{-1}; Mazzali et al. 1998).

4.4 Violent white dwarf mergers

Pakmor et al. (2010, 2011) considered "violent" mergers of two carbon-oxygen white dwarfs, in which the explosion happens promptly during the dynamical merger process, as progenitors of peculiar, subluminous SNe Ia. Later, Pakmor et al. (2012) presented a new violent merger model with $M_{\mathrm{Ni}} = 0.6$ $M_\odot$, capable of representing a normal SN Ia. The findings of these simulations suggested that the mass of the primary white dwarf was the most important parameter determining ^{56}Ni production, since the less massive secondary is totally disrupted in the explosion and its remnants do not achieve high enough densities to burn to the iron peak. Operating on this assumption, Ruiter et al. (2013) used binary population synthesis models to predict the distribution of M_{Ni} for violent mergers, comparing to the observed absolute magnitude distribution from Li et al. (2011). They found the predicted distribution to be more or less peaked around $M_{\mathrm{Ni}} \sim 0.6$ $M_\odot$ ($M_{\mathrm{ej}} \sim 1.1$ $M_\odot$), depending on assumptions about the mass ratio necessary to ignite a detonation in the primary white dwarf.

The physical explosion mechanism in the Pakmor et al. (2012) violent mergers is similar to that in a double detonation, and the parameter space is approximately bounded from below by the Fink et al. (2010) curve in our Figure 1. However, M_{ej} could vary significantly from system to system, depending on the fate of the secondary. If the secondary is always completely disrupted (as in

Pakmor et al. 2010, 2011, 2012), then M_{ej} will be significantly higher for given M_{Ni} than in double detonation models, but may still vary from system to system because of differences in the secondary mass. Even more variation in the total mass could occur if only a portion of the secondary mass is unbound, which may be possible in some cases. The conclusion of Scalzo et al. (2014a) that violent mergers could not explain most normal SNe Ia was based on the assumption that a mass ratio greater than 0.8 was necessary for ignition, and that the entire mass of the system was ejected in the explosion, as in Pakmor et al. (2012). However, no comprehensive parameter studies for the fate of the secondary star in this scenario have yet been made. In particular, much of the material from the disrupted secondary star may lie at low velocities (Pakmor et al. 2012; Röpke et al. 2012; Kromer et al. 2013b), in tension with late-time observations of normal SNe Ia (but see Kromer et al. 2013a).

In a separate study, Moll et al. (2014) performed three-dimensional simulations of three different violent mergers. In these models, M_{Ni} also varies with M_{ej}, though with a different functional dependence than that predicted by Ruiter et al. (2013); the ejecta are highly aspherical, even toroidal, and the light curve varies strongly with viewing angle. The effective α, relative to spherical models such as Arnett (1982), lie in the range 0.6–1.7, clearly violating Arnett's rule; the 1.95-$M_\odot$ merger model of Pakmor et al. (2012) showed similar variation between different lines of sight. Similar variation could in principle produce the narrow light curves seen by Scalzo et al. (2014a) for the SNe Ia they infer to be the least massive, particularly SN 2005el, which presented the most tension with expectations from spherical models. However, all of the Moll et al. (2014) mergers are brighter at late times than SN 2005el, or indeed most of the Scalzo et al. (2014a) bolometric light curves. Moreover, the brighter lines of sight tend to have narrower bolometric light curves, whereas Scalzo et al. (2014a) find the opposite trend, indicating that asymmetry is unlikely to be the sole source of diversity in bolometric light curves.

Pakmor et al. (2013) suggested that the violent merger scenario could be extended to include mergers of a carbon-oxygen white dwarf with a helium white dwarf, making detonations easier to achieve and lowering the overall ejected mass. One important property that determines whether a double-degenerate system will merge is the mass ratio: more similar masses are likely to merge, less similar masses are more likely to undergo (non-dynamical) stable Roche lobe overflow. Since helium white dwarf masses lie in a narrower mass range and are less massive compared to carbon-oxygen white dwarfs, the systems that do merge will occur in the low-mass end of the primary's mass distribution, so their masses/densities will be too low to satisfy the criteria needed for a SN Ia explosion. Systems with carbon-oxygen WD masses that *are* large enough to synthesize enough ^{56}Ni in the explosion tend to be found among non-merging populations (those with stable mass transfer; see Figure 2 of Ruiter et al. 2014). However, the conditions typically assumed to lead to a merger in binary population synthesis codes may be too conservative (e.g., Toonen et al. 2014). Merger scenarios between carbon-oxygen and helium-rich WDs indeed warrants further exploration (e.g. Dan et al. 2012), since such scenarios may further expand the allowed parameter space for violent mergers, or pick out particular regions of interest.

In principle, variations in the fraction of the secondary's mass ejected, or in the amount of ^{56}Ni produced in a dynamical merger (Zhu et al. 2013; Dan et al. 2013), allow violent mergers to occupy the entire M_{ej}-M_{Ni} plane above the Fink et al. (2010) double-detonation boundary shown in Figure 1. The challenge for violent merger models is then to explain why more SNe Ia are *not* ob-

served far from the locus of points corresponding to the familiar width-luminosity relation.

4.5 White dwarf collisions

Collisions of two white dwarfs (Benz et al. 1989) have been suggested as a means to produce SNe Ia. Except in very dense environments such as globular clusters, the rate of white dwarf collisions is expected to be very low. However, Kozai resonances in triple systems can decrease the delay time to a collision to increase the rate of SNe Ia from these systems (Thompson et al. 2011; Katz & Dong 2012; Hamers et al. 2013). Simulations have shown that explosion will occur following collision (Rosswog et al. 2009; Raskin et al. 2010; Kushnir et al. 2013), and calculations of light curves and spectra suggest that reasonable agreement with observations of normal SNe Ia may be possible (Rosswog et al. 2009). Furthermore, Dong et al. (2014) present a sample of nebular spectra of SNe Ia that show double-peaked line profiles, which they interpret as evidence for axisymmetric (but aspherical) explosions characteristic of white dwarf collisions.

This scenario shares many of the attractive qualities of the violent merger scenario: compared to the double-detonation scenario, the collision model predicts higher M_{ej} (for given M_{Ni}), and can accomodate a significant range of ejected mass by allowing for variation in the mass ratio of the colliding pair (Kushnir et al. 2013). However, due to large uncertainties in the distribution of properties of triple systems, this scenario currently makes no definite prediction for the expected absolute rate of collision events, for the distribution of masses of the colliding white dwarfs, or for the aggregate delay time distribution of white dwarf collisions. The only predictions currently made for these models are positions in the M_{ej}-M_{Ni} plane.

We see in Figure 1 that the models of Kushnir et al. (2013) lie close to some of our slower-declining SNe Ia. Interestingly, the cosmological width-luminosity relation intersects the M_{ej}-M_{Ni} relation for equal-mass white dwarf collisions near $M_{\mathrm{ej}} = 1.4\ M_{\odot}$. However, none of the current Kushnir et al. (2013) collision models appear in the correct region of the M_{ej}-M_{Ni} plane to reproduce the fastest-declining normal SNe Ia. There are also several merger models on the high-mass, slow-declining end that are not realized in the observations.

As in the discussion of double detonations, a calibration error of 0.2 $M_{\odot}$ in our M_{ej} estimates could in principle shift the entire M_{ej}-M_{Ni} distribution up by 0.2 $M_{\odot}$, which would improve the correspondence between the full range of SNe Ia we observe and a subset of the Kushnir et al. (2013) unequal-mass white dwarf collisions. There is no particular motivation to do this on naturalness grounds, however: without predictions for relative rates of collisions between white dwarfs of different masses and mass ratios, we have no compelling reason to prefer any subset of these models to any other subset.

5 CONCLUSIONS

We have estimated ^{56}Ni masses and ejected masses for a large sample of normal SNe Ia, carefully selected to be unbiased with respect to their host galaxy environments and explosion parameters. The estimates are based on empirical relations derived from the more detailed bolometric light curve modeling of Scalzo et al. (2014a). Applying hierarchical Bayesian inference to this sample, we have derived the intrinsic joint distribution between ^{56}Ni mass and ejected mass in SNe Ia, finding that it closely follows the empirical one-parameter SN Ia width-luminosity relation. At least one-

quarter of normal SNe Ia are sub-Chandrasekhar-mass at high confidence, and the rate may be as high as one-half. The fraction of normal SNe Ia with super-Chandrasekhar-mass ejecta appears to be quite small, about 1%.

While our distribution is not obviously bimodal, we find that its properties cannot be adequately described by any single explosion model. The main constraints can be summarized as follows:

(i) *Chandrasekhar-mass models:* These explain many SNe Ia well. However, to match bolometric light curves in the fastest-declining quartile of normal SNe Ia, Chandrasekhar-mass models must show a narrow bolometric light curve typical of short diffusion times, while emitting substantially more radiation around maximum light than generated by radioactivity. These features do not seem to be supported by contemporary Chandrasekhar-mass explosion models.

(ii) *Double detonations:* These explain some fast-declining SNe Ia well, but (as pure detonations) produce too much ^{56}Ni to explain normal SNe Ia outside of a narrow range of ejected masses.

(iii) *Violent white dwarf mergers:* These have the potential to explain a wide range of ^{56}Ni masses and ejected masses, depending on how efficiently they synthesize ^{56}Ni and how much mass they eject. It remains to be seen whether the width-luminosity relation can be explained as a consequence of the details of the merger dynamics or population synthesis; more research is needed to make definite predictions.

(iv) *White dwarf collisions:* The best existing models fit observed Chandrasekhar-mass explosions well, but not most sub-Chandrasekhar-mass explosions, unless the calibration of our method is quite wrong. As with violent mergers, our observed distribution could place constraints on which actual systems can collide to form SNe Ia.

As a caveat, white dwarf mergers and collisions are expected to be highly aspherical. This explicitly breaks the approximation of spherical symmetry used in Scalzo et al. (2014a), and may give rise to line-of-sight effects that cause the true values of M_{ej} and M_{Ni} to deviate from our estimates to some extent. However, these effects should tend to increase diversity rather than decreasing it, and there are observational reasons (e.g., polarization) to believe that asymmetries are modest rather than extreme. There is thus no compelling reason to believe that asymmetry plays a major role, unless it drives a low-scatter width-luminosity relation within the context of a specific scenario.

In fact, the full M_{ej}-M_{Ni} distribution is currently beyond the capacity of any single explosion model or progenitor scenario to predict, owing partly to challenges in modeling explosions and partly to challenges in modeling stellar populations. As theoretical predictions improve, our distribution will provide strong constraints on the entire end-to-end physical processes resulting in SNe Ia, from initial formation of the system through to the final explosion. Our methodology is simple, relying only on photometry that will be collected for any SN Ia cosmology experiment, and can be repeated in the future with much larger data sets, such as those provided by the Dark Energy Survey (DES) and Large Synoptic Survey Telescope (LSST). With enough events from untargeted surveys at both low and high redshifts, the delay time t_{delay} can also be folded in, enabling comparison of end-to-end modeling to the full *trivariate* M_{ej}-M_{Ni}-t_{delay} distribution. Such complete information about the distributions of progenitor properties could allow us not only to determine, authoritatively, which progenitor and explosion channels contribute to SNe Ia, but in what proportions and in what regions of parameter space, enabling new breakthroughs both in cosmology and in stellar evolution.

ACKNOWLEDGMENTS

REFERENCES

Arnett, W. D. 1982, ApJ, 253, 785
Anand, S. P. S. 1965, Proc. Natl. Acad. Sci., 54, 23
Astier, P., Guy, J., Regnault, N., et al. 2006, ApJ, 447, 31
Bailey, S., Aldering, G., Antilogus, P., et al. 2009, A&A, 500, L17
Baron, E., Höflich, P., Krisciunas, K., et al. 2012, ApJ, 753, 105
Betoule, M., Kessler, R., Guy, J., et al. 2014, A&A, submitted (arXiv:1401:4064)
Benz, W., Thielemann, F.-K., & Hills, J. G. 1989, ApJ, 342, 986
Blinnikov, S. I. & Sorokina, E. I. 2010, arXiv:1009.4353
Bloom, J. S., Kasen, D., Shen, K. J., et al. 2012, ApJ, 744, L17
Blondin, S., Matheson, T., Kirshner, R. P., et al. 2012, AJ, 143, 5
Blondin, S., Dessart, L., Hillier, D. J., et al. 2013, MNRAS, 429, 2127
Bongard, S., Baron, E., Smadja, G., et al. 2006, ApJ, 647, 513
Branch, D., Fisher, A., & Nugent, P. 1993, AJ, 106, 2383
Branch, D., Dang, L., Hall, N., et al. 2006, PASP, 118, 560
Branch, D., Troxel, M. A., Jeffery, D. J., et al. 2007, PASP, 119, 135
Branch, D., Jeffery, D. J., Parrent, J., et al. 2008, PASP, 120, 135
Burns, C., Stritzinger, M., Phillips, M. M., et al. 2014, ApJ, in press (arXiv:1405.3934)
Cardelli, J. A., Clayton, G. C. & Mathis, J. S. 1988, ApJ, 329, L33
Chamulak, D. A., Brown, E. F., Timmes, F. X., et al. 2008, ApJ, 677, 160
Chotard, N., Gangler, E., Aldering, G., et al. 2011, A&A, 529, 4
Churazov, E., Sunyaev, R., Isern, J., et al. 2014, arXiv:1405.3332
Conley, A., Goldhaber, G., Wang, L., et al. 2006, ApJ, 644, 1
Dan, M., Rosswog, S., Guillochon, J., et al. 2012, MNRAS, 422, 2417
Dan, M., Rosswog, S., Brüggen, M., et al. 2014, MNRAS, 438, 14
Di Stefano, R. 2010, ApJ, 712, 728
Di Stefano, R. 2010, ApJ, 719, 474
Di Stefano, R. & Kilic, M. 2012, ApJ, 759, 56
Dong, S., Katz, B., Kushnir, D., et al. 2014, arXiv:1401.3347
Fink, M., Röpke, F. K., Hillebrandt, W., et al. 2010, A&A, 514, A53
Filippenko, A. V., Richmond, M. W., Matheson, T., et al. 1992, ApJ, 384, L15
Fink, M., Kromer, M., Seitenzahl, I. R., et al. 2014, MNRAS, 438, 1762
Folatelli, G., Phillips, M. M., Burns, C., R., et al. 2010, AJ, 139, 120
Foley, R. J. & Kasen, D. 2010, ApJ, 729, 55
Foreman-Mackey, D., Hogg, D. W., Lang, D., et al. 2013, PASP, 125, 306
Frieman, J. A., Bassett, B., Becker, A., et al. 2008, AJ, 135, 338
Fryer, C. L., Ruiter, A. J., Belczynski, K., et al. 2010, ApJ, 725, 296
Goldhaber, G., Groom, D. E., Kim, A. G., et al. 2001, ApJ, 558, 359
Gilfanov, M. & Bogdán, Á. 2010, Nature, 463, 924
Guy, J., Astier, P., Baumont, S., et al. 2007, A&A, 466, 11
Guy, J., Sullivan, M., Conley, A., et al. 2010, A&A, 523, 7
Hachisu, I., Kato, M., Saio, H., et al. 2012, ApJ, 744, 69
Hamers, A. S., Pols, O. R., Claeys, J. S. W., et al. 2013, MNRAS, 430, 2262
Hicken, M., Garnavich, P. M., Prieto, J. L., et al. 2007, ApJ, 669, L17
Hillebrandt, W., Kromer, M., Röpke, F. K., & Ruiter, A. J. 2013, Frontiers of Physics, 8, 116
Höflich, P. & Khokhlov, A. 1996, ApJ, 457, 500
Höflich, P., Gerardy, C., Nomoto, K., et al. 2004, ApJ, 617, 1258
Hogg, D., Myers, A., & Bovy, J. 2010, ApJ, 725, 2166
Howell, D. A., Sullivan, M., Nugent, P. E., et al. 2006, Nature, 443, 308
Howell, D. A. et al. 2007, ApJ, 667, 37
Howell, D. A. et al. 2009, ApJ, 691, 661
Iben, I. & Tutukov, A. V. 1984, ApJS, 54, 335
Iben, I. & Tutukov, A. V. 1991, ApJ, 370, 615
Jha, S., Branch, D., Chornock, R., et al. 2006, AJ, 132, 189
Jordan, G. C., Perets, H. B., Fisher, R. T., et al. 2012, ApJ, 761, L23

Justham, S. 2011, ApJ, 730, L34
Kasen, D., Röpke, F. K., & Woosley, S. E. 2009, Nature, 460, 869
Katz, B. & Dong, S. 2012, arXiv:1211.4584
Khokhlov, A. 1991, A&A, 245, 114
Khokhlov, A., Müller, E. & Höflich, P. 1993, A&A, 270, 223
Krisciunas, K., Li, W., Matheson, T., et al. 2011, AJ, 142, 74
Kromer, M., Fink, M., Stanishev, V., et al. 2013, MNRAS, 429, 2287
Kromer, M., Pakmor, R., Taubenberger, S., et al. 2013, ApJ, 778, 18
Krueger, B. K. Jackson, A. P., Townsley, D. M., et al. 2012, ApJ, 757, 175
Kushnir, D., Katz, B., Dong, S., et al. 2013, ApJ, 778, L37
Li, W., Leaman, J.; Chornock, R., et al. 2011, MNRAS, 412, 1441
Livne, E., Asida, S. M., & Höflich, P. 2005, ApJ, 632, 443
Lesaffre, P., Han, Z., Tout, C. A., et al. 2006, MNRAS, 368, 187
Long, M., Jordan, G. C., van Rossum, D. R., et al. 2013, arXiv:1307.8221
Maeda, K., Leloudas, S., Taubenberger, S., et al. 2011, MNRAS, 413, 3075
Mandel, K. S., Wood-Vasey, W. M., Friedman, A. S., et al. 2009, ApJ, 704, 629
Mandel, K. S., Narayan, G., & Kirshner, R. P. 2011, ApJ, 731, 120
Mannucci, F., Della Valle, M., Panagia, N. 2006, MNRAS, 370, 773
Mazzali, P. A., Cappellaro, E., Danziger, I. J., et al. 1998, ApJ, 499, L49
Mazzali, P. A., Röpke, F., Benetti, S., et al. 2007, Science, 315, 825
Mazzali, P. A., Maurer, I., Stritzinger, M., et al. 2011, MNRAS, 416, 881
Mazzali, P. A., & Hachinger, S. 2012, MNRAS, 424, 2926
Moll, R., Raskin, C., Kasen, D., et al. 2014, ApJ, 785, 105
Motohara, K., Maeda, K., Gerardy, C. L., et al. 2006, ApJ, 652, L101
Nomoto, K. & Kondo, Y. 1991, ApJ, 367, L19
Nugent, P., Branch, D., Baron, E., et al. 1995, Phys. Rev. Lett., 75, 394
Nugent, P., Sullivan, M., Cenko, S. B., et al. 2011, Nature, 480, 344
Pakmor, R., Kromer, M., Röpke, F. K., et al. 2010, Nature, 463, 61
Pakmor, R., Hachinger, S., Röpke, F. K., et al. 2011, A&A, 528, 117
Pakmor, R., Kromer, M., & Taubenberger, S. 2013, ApJ, 747, L10
Pakmor, R., Kromer, M., Taubenberger, S., et al. 2013, ApJ, 770, L8
Perlmutter, S., Aldering, G., Goldhaber, G., et al. 1999, ApJ, 517, 565
Phillips, M. M., Wells, L. A., Suntzeff, N. B., et al. 1992, AJ, 103, 1632
Phillips, M. M. 1993, ApJ, 413, 105
Phillips, M. M., Lira, P., Suntzeff, N. B., et al. 1999, AJ, 118, 1766
Phillips, M. M., Li, W., Frieman, J. A., et al. 2007, PASP, 119, 360
Pinto, P. & Eastman, R. 2000, ApJ, 530, 744
Piro, A. 2008, ApJ, 679, 616
Piro, A., Chang, P., & Weinberg, N. N. 2010, ApJ, 708, 598
Piro, A., Thompson, T. A., & Kochanek, C. S. 2014, MNRAS, 438, 3456
Raskin, C., Timmes, F. X., Scannapieco, E., et al. 2009, MNRAS, 399, L156
Raskin, C., Scannapieco, E., Rockefeller, G., et al. 2010, ApJ, 724, 111
Riess, A. G., Press, W. H., & Kirshner, R. P. 1996, ApJ, 473, 88
Riess, A. G., Filippenko, A. V., Challis, P., et al. 1998, AJ, 116, 1009
Röpke, F. K., Kromer, M., Seitenzahl, I. R., et al. 2012, ApJ, 750, 19
Rosswog, S., Kasen, D., Guillochon, J., et al. 2009, ApJ, 705, 128
Roxburgh, I. W. 1965, Z. Astrophys., 62, 134
Ruiter, A. J., Sim, S. A., Pakmor, R., et al. 2013, MNRAS, 429, 1425
Ruiter, A. J., Belczynski, K., Sim, S. A., et al. 2014, MNRAS, 440, L101
Ruiz-Lapuente, P. 2014, New Ast. Rev., submitted (arXiv:1403.4087)
Sahu, D. K., Tanaka, M., Anupama, G. C., et al. 2008, ApJ, 680, 580
Scannapieco, E., & Bildsten, L. 2005, ApJ, 629, 85
Scalzo, R. A., Aldering, G., Antilogus, P., et al. 2010, ApJ, 713, 1073
Scalzo, R. A., Aldering, G., Antilogus, P., et al. 2012, ApJ, 757, 12
Scalzo, R. A., Aldering, G., Antilogus, P., et al. 2014, MNRAS, 440, 1498
Scalzo, R. A., Childress, M., Tucker, B., et al. 2014, MNRAS, submitted (arXiv:1404.1002)
Scolnic, D., Riess, A., Foley, R. J., et al. 2014, ApJ, 780, 1
Seitenzahl, I., Ciaraldi-Schoolmann, F., & Röpke, F. K. 2011, MNRAS, 414, 2709
Seitenzahl, I., Ciaraldi-Schoolmann, F., Röpke, F. K., et al. 2013, MNRAS, 429, 1156
Seitenzahl, I., Cescutti, G., Röpke, F. K., et al. 2013, A&A, 559, L5
Sim, S. A., Röpke, F. K., Hillebrandt, W., et al. 2010, ApJ, 714, L52
Sim, S. A., Seitenzahl, I. R., Röpke, F. K., et al. 2013, MNRAS, 436, 333
Shen, K., Bildsten, L., Kasen, D., et al. 2012, ApJ, 748, 35
Stehle, M., Mazzali, P. A., Benetti, S., et al. 2005, MNRAS, 360, 1231

Stritzinger, M., Leibundgut, B., Walch, S., et al. 2006, A&A, 450, 241

Sullivan, M., Le Borgne, D., Pritchet, C. J., et al. 2006, ApJ, 648, 868

Tanaka, M., Kawabata, K., Yamanaka, M., et al. 2010, ApJ, 714, 1209

Taubenberger, S., Benetti, S., Childress, M. et al. 2011, MNRAS, 412, 2735

Taubenberger, S., Kromer, M., Hachinger, S. et al. 2013, MNRAS, 432, 3117

Thompson, T. A. 2011, ApJ, 741, 82

Toonen, S., Claeys, J. S. W., Mennekens, N., et al. 2014, A&A, 562, 14

Tripp, R. 1998, A&A, 331, 815

van Kerkwijk, M., Chang, P., & Justham, S. 2010, ApJ, 722, L157

Wang, B., & Han, Z. 2012, New Astronomy Reviews, 56, 122

Wang, L., & Wheeler, J. C. 2008, ARA&A, 46, 433

Wang, X., Filippenko, A. V., Ganeshalingam, M., et al. 2009, ApJ, 699, L139

Whelan, J. & Iben, I. J. 1973, ApJ, 186, 1007

Woods, T. E., & Gilfanov, M. 2013, MNRAS, 432, 1640

Woosley, S. E. & Weaver, T. A. 1994, ApJ, 423, 371

Woosley, S. E. & Kasen, D. 2007, ApJ, 662, 487

Woosley, S. E. & Kasen, D. 2011, ApJ, 734, 38

Yamanaka, M., Kawabata, K., Kinugasa, K., et al. 2009, ApJ, 707, L118

Yoon, S.-C. & Langer, N. 2005, A&A, 435, 967

Yuan, F., Quimby, R. M., Wheeler, J. C., et al. 2010, ApJ, 715, 1338

Zhu, C., Chang, P., van Kerkwijk, M., et al. 2013, ApJ, 767, 164